J. Phys. F: Met. Phys. **14** (1984) 281–290. Printed in Great Britain

Spin–orbit and crystal-field effects in AgPt dilute alloys

D van der Marel†, G A Sawatzky† and J A Julianus‡

† Physical Chemistry Department of the Material Science Center, University of Groningen, Nijenborgh 16, 9747 AG Groningen, The Netherlands

‡ Natuurkundig Laboratorium, University of Amsterdam, Valckenierstraat 65, 1018 XE Amsterdam, The Netherlands

Received 31 May 1983, in final form 25 July 1983

Abstract. High-resolution photoemission spectra are presented of Ag–1.90 at% Pt and Ag–10 at% Pt alloys, together with low-temperature thermopower measurements on Ag–1.05 at% Pt and Ag–1.28 at% Pt samples. The photoemission data clearly show a splitting of the virtual bound Pt 5d states due to spin–orbit and crystal-field effects. A simple atomic theory, including these effects, is presented and shown to fit the photoemission data. The spin–orbit coupling is found to be only slightly reduced from the spectroscopic free-atom value. We show that the virtual bound state parameters extracted from the photoemission spectra can describe the experimental transport data within a free-electron phase-shift model incorporating only spin–orbit coupling. It is found to be necessary to include s and p phase shifts.

1. Introduction

AgPt and **Ag**Pd alloys are examples of virtual bound state (VBS) systems in which the impurity d states are not split by exchange interactions and are energetically situated between the Ag 4d band and the Fermi level (Hüfner *et al* 1975, Weightman *et al* 1983, Smith 1981). As part of a more extended study of Pt, Pd and Ni impurities in metals we report here a high-resolution UPS and electron transport study of **Ag**Pt. This system is interesting because firstly the Pt VBS is clearly visible on top of the structureless Ag sp band, and secondly the VBS is expected to be quite narrow so that spin–orbit and crystal-field splittings should be clearly visible. Recent XPS (Hüfner *et al* 1975) and theoretical studies (Smith 1981) have indicated that high-resolution spectra should facilitate a detailed analysis of spin–orbit and crystal-field effects.

In this paper we present experimental UPS and thermopower data for some **Ag**Pt alloys (dilute limit and 10 at%) and we analyse the UPS data in terms of a VBS theory in which exact expressions are used for the spin–orbit and crystal-field effects in cubic symmetry. It should be noted that the expressions given by Smith (1981) for the energies of the Γ_7 and Γ_8 representations are valid only in the large crystal-field limit which we will show is not applicable to **Ag**Pt. Also we show that in the 10 at% alloy the VBS is strongly broadened, presumably due to Pt–Pt interactions. The low-temperature thermopower measurements together with resistivity data are analysed in a free-electron phase-shift model including

0305-4608/84/010281 + 10 $02.25

spin–orbit effects. The positions and widths of the VBS are deduced from the UPS spectra and used as input parameters in this analysis.

2. Sample preparation

The 10 at% Pt alloy was made by arc melting and was annealed for three days at 800 °C to homogenise. The other samples were prepared at the University of Leeds by melting weighed quantities of the components in a sealed quartz tube. This was quenched in water and the alloy was then rolled and etched until the required diameter (1×1 mm^2) was reached. The resistivity was measured, to check the homogeneity of the samples, by a standard four-probe method before and after the rods were annealed at about 800 °C and quenched in water. The samples (except the 10 at% Pt alloy) were analysed with the atomic absorption spectrophotometry technique using an air–acetylene flame. The wire samples for the thermoelectric force (TEF) measurements were drawn from the annealed rods in diamond dies to a diameter of 0.25 mm. The resistivities given in table 1 are those of the rods from which the wires were drawn. The 1.90 at% Pt strip for the UPS measurements was rolled from the annealed rod.

3. Experimental technique

3.1. UPS

Data were collected with a modified PHI double-pass cylindrical mirror analyser which is designed for simultaneous angular resolved photoemission (Bosch 1982). In this paper we use the system in an angular integrated mode. The measurements were made at 10 eV pass energy with a resolution of 85 meV, as determined from Ar gas phase measurements. The transmission was also greatly improved so that measurements on 2 at% alloys are easily made. The samples were mechanically polished before insertion in the vacuum chamber and subsequently etched with 1 keV Ar ions. The etching was repeated every 30 min, after which time the spectrum had not noticeably deteriorated due to surface contamination.

3.2. Thermopower

The cryostat used for the TEF measurements is described by Bekker and Hoogkamer (1976). The technique used is the integral method, i.e. the TEF

$$E_{T_b}^{T} = \int_{T_b}^{T} S \, \mathrm{d}T$$

is measured as a function of temperature T, while T_b is kept constant. The TEF of the sample is measured against a superconducting Nb_3Sn reference strip over the temperature range 1.5–16 K. Spurious thermoelectric effects are eliminated through a superconducting switch of the heater-controlled type. A balancing current through a known resistor ($R_b = 0.468$ mΩ), at helium bath temprature, is adjusted to compensate the TEF of the sample which enables an accuracy of typically 1 nV. A Keithley 148 nanovoltmeter is used as null-detector.

4. Results and analysis

4.1. Analysis of UPS spectra

The spectra shown are accumulations of single sweeps (approximately 4 min per sweep) resulting in a total of 10^5 counts in the most intense channels.

In figure 1 the spectra are shown for pure Ag and for the 1.90 at% and 10 at% Pt alloys. The Pt 5d peaks in the 1.90 at% alloy are clearly visible between the Ag 4d band and the Fermi level. In addition to these peaks, structure in the Ag 4d band region is also changed due to alloying. In a subsequent paper on Pt and Pd alloys we will discuss this part of the spectrum. In this paper we concentrate on the extra structure between the Ag 4d band and the Fermi level, which should provide information on the spin–orbit coupling and crystal-field splitting.

In figure 2 the difference spectra are shown for an energy region up to 3.5 eV below the Fermi level. In the 1.90 at% alloy we clearly see two peaks at about 2.65 eV and 1.6 eV below the Fermi level. The peak at about 1.6 eV is considerably broader; we show below that this is a direct consequence of the crystal-field splitting. The 10 at% alloy also shows structure but this is strongly broadened and also shifted relative to the 'dilute' alloy. A similar shift was observed by Hüfner *et al* (1975) in XPS measurements of Ag–5 at% Pt and Ag–10 at% Pt alloys. The changes with increasing Pt concentration are probably a result of Pt–Pt contacts. For a random 10 at% alloy, for example, the probability that a Pt atom has one or more nearest neighbours is 72%, whereas for the 1.90 at% alloy it is only 12% for a FCC lattice.

From the above we expect that the 1.90 at% alloy spectrum can be analysed according to dilute alloy theory. We consider the Pt 5d states to be embedded in the sp band of Ag. We neglect for now the interactions with the Ag 4d states. This interaction is not in fact

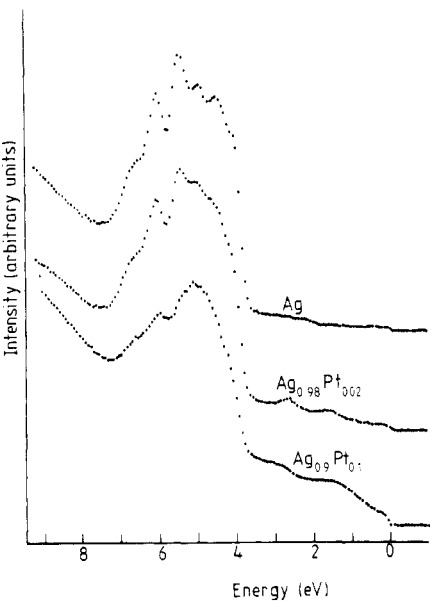

Figure 1. UPS valence band spectra of pure Ag and the Ag–1.90 at% Pt and Ag–10 at% Pt alloys.

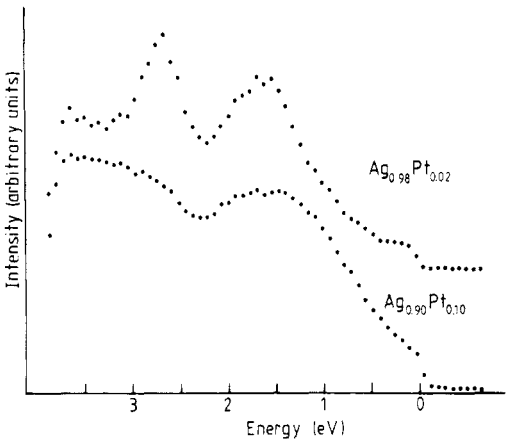

Figure 2. Difference spectra (alloy – pure Ag) for the Ag–1.90 at% Pt and Ag–10 at% Pt alloys.

negligible but as we will show in a subsequent paper (van der Marel *et al* 1984) it does not strongly affect the width or splittings of the peaks.

To describe the difference spectra in terms of spin–orbit coupling, crystal-field splitting and hybridisation with the Ag sp band, we assume that the difference spectrum is proportional to the Pt 5d local density of states. This is justified because the Ag sp band density of states is quite flat in this energy region, so it will hardly change upon alloying, and also the photoemission cross section for the Pt 5d electrons for He I radiation is orders of magnitude larger than that for Ag sp electrons.

We first consider the Pt 5d one-electron states including spin–orbit coupling and a cubic crystal-field splitting. In the O_h double group the irreducible representations spanned by the states of a d electron are Γ_7, Γ_8 and $\Gamma_{8'}$, which are twofold and fourfold degenerate, respectively. Neglecting first the spin–orbit coupling, the irreducible representations in crystal-field notation are then $\Gamma_7(t_{2g})$, $\Gamma_8(t_{2g})$ and $\Gamma_8(e_g)$. The spin–orbit interaction has matrix elements given by (Ballhausen 1962)

$$H_{SO}\Gamma_8^n(t_{2g}) = -\tfrac{1}{2}\xi\Gamma_8^n(t_{2g}) + \xi\sqrt{3/2}\Gamma_8^n(e_g)$$

$$H_{SO}\Gamma_7^n(t_{2g}) = \xi\Gamma_7^n(t_{2g})$$

$$H_{SO}\Gamma_8^n(e_g) = \xi\sqrt{3/2}\Gamma_8^n(t_{2g})$$

resulting in energies

$$E(\Gamma_7) = -4Dq + \xi$$

$$E(\Gamma_8) = Dq - \tfrac{1}{4}\xi \pm \tfrac{1}{2}[(10Dq + \tfrac{1}{2}\xi)^2 + 6\xi^2]^{1/2}$$

where $10Dq$ is the crystal-field splitting parameter and ξ is the spin–orbit coupling constant. In figure 3 the energies for the three representations are shown for $\xi = 0.39$ eV as functions of $10Dq$.

The interpretation of the experimental spectrum (which differs strongly from the theoretical spectrum of Smith (1981)) now becomes clear. The broader, and in total more intense, structure at 1.6 eV must involve in total more states than the peak at 2.65 eV, suggesting an assignment to the upper Γ_7 and $\Gamma_{8'}$ states of figure 3. It should be noted that the extra broadening could not be due to a surface component shifted in energy since then

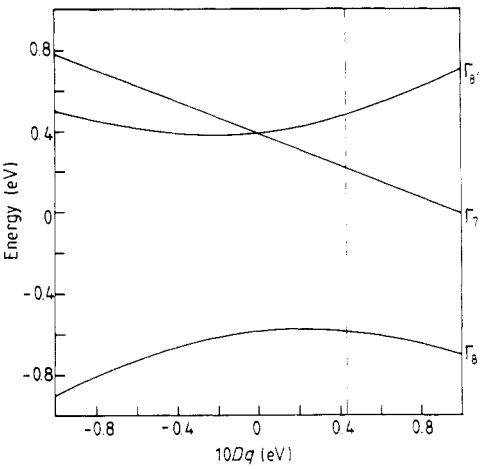

Figure 3. Calculated splitting of the Γ_7, Γ_8 and $\Gamma_{8'}$ levels with a spin–orbit coupling ξ of 0.39 eV as a function of the crystal-field splitting parameter. The broken line shows approximately the experimental value of the crystal-field splitting.

and also the photoemission cross section for the Pt 5d electrons for He I radiation is 2.65 eV must then originate from the lower Γ_8 state of figure 3. We obtain a satisfactory fit taking $10Dq = 0.43$ eV and $\xi = 0.39$ eV, splitting the broader structure into two peaks at 1.50 and 1.80 eV. The screening charges obtained by integrating the Lorentzians up to ε_F are 3.89, 1.92 and 3.81 for Γ_8, Γ_7 and $\Gamma_{8'}$, respectively. Figure 4 shows the theoretical curve for the above parameters assuming a Lorentzian line shape for each component with a full width at half maximum (FWHM) of 0.45 eV and intensity proportional to the degeneracy. The separate contributions of the three components are also shown. For comparison with the experimental spectrum, a linear background was added to the calculated spectrum to account for inelastically scattered electrons.

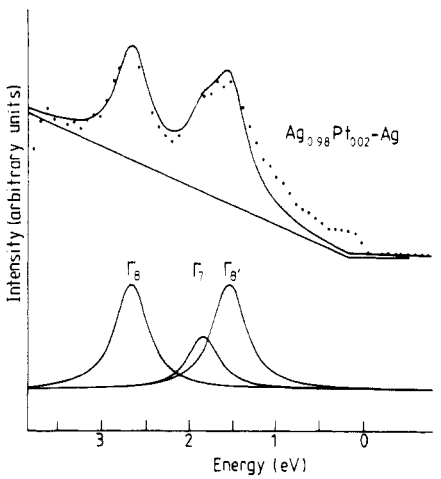

Figure 4. Comparison of the experimental (dots) 1.90 at% alloy data with the theoretically simulated spectrum (full curve). Also shown are the separate contributions of the three irreducible representations. The parameters used are $\xi = 0.39$ eV, $10Dq = 0.43$ eV and FWHM = 0.45 eV.

Table 1. Analysis of TEF measurements. A, B and C are the least-squares fitting parameters in equation (1). The fits are made up to $T=\theta$ of N_θ data points and σ_θ is the standard deviation.

c (at% Pt)	ρ ($\mu\Omega$ cm)	θ_{max} (K)	A (nV K^{-2})	B (nV K^{-4})	C (nV K^{-1})	σ_θ	N_θ
1.05 ± 0.02	1.49	10	−13.04 ± 0.04		−14.5 ± 0.2	0.73	44
1.28 ± 0.03	1.78	8	$-14.4_3 \pm 0.1$	0.022 ± 0.004		1.39	30

We see that the main features of the spectrum are well represented by the simple 'quasi-atomic' theory. The discrepancy observed close to the Fermi level may be due, at least in part, to Pt atoms with Pt nearest neighbours. In comparing with the 10 at% alloy (figure 2) we observe that the relative intensity close to the Fermi level increases with an increase in the number of Pt–Pt contacts.

The observed spin–orbit coupling is only slightly smaller than the spectroscopic value (0.42 eV) found for Pt (Moore 1949). A small reduction is expected because of the mixing with the Ag 4d band, which causes a larger shift towards the Fermi level of the 3/2 component than of the 5/2 component.

The crystal-field splitting is a factor of ten larger than the values Smith (1974) found for Pt metal (0.023 eV) by means of interpolation. In both cases $10Dq$ is positive, which places the e_g levels closer to the Fermi level than the t_{2g}. It should be noted that changing the sign of $10Dq$ would place the twofold Γ_7 level closer to the Fermi level than the Γ_8 level and this would not fit the experimental spectrum.

4.2. *Analysis of TEF measurements*

The absolute thermoelectric power (TEP) of noble-metal-based dilute alloys can usually be adequately described by a formula of three terms:

$$S = AT + BT^3 + C\frac{T}{T+T_0}. \tag{1}$$

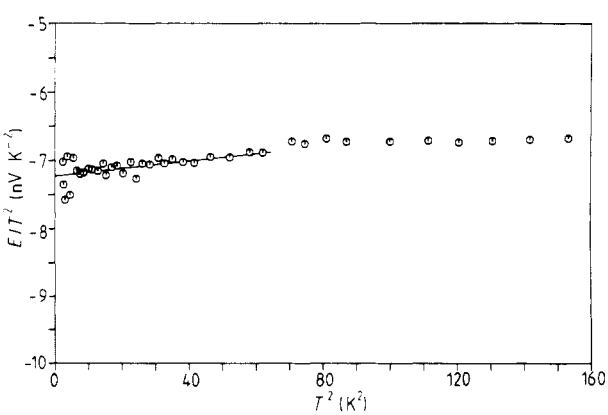

Figure 5. Illustration of the phonon drag term in the TEF of the Ag–1.28 at% Pt alloy. The full line is the least-squares fit up to 8 K. The intercept and the slope of the curve give the values $\frac{1}{2}A$ and $\frac{1}{4}B$ in equation (1) ($C=0$), respectively.

Our main interest is in the electron diffusion term (AT). The second and third terms describe the phonon drag and the scattering at magnetic (iron) impurities (Kondo 1965), respectively. The value for $T_0(=0.15\ \mathrm{K})$ is adopted from Guénault (1967). The TEF data points were fitted to the integral expression of equation (1). The results of the least-squares fit are summarised in table 1. A small B term is observed in the 1.28 at% Pt alloy (figure 5).

There is some ambiguity about the ρ/c value for **Ag**Pt. The experimental value for the resistivity has been reviewed recently by Bass and Fischer (1982), who analysed earlier measurements of Barber and Caplin (1975). The result was $\rho/c = 1.32\ \mu\Omega\ \mathrm{cm\ (at\%)^{-1}}$. However, Myers (private communication) reports a value of $1.42\ \mu\Omega\ \mathrm{cm\ (at\%)^{-1}}$ based on chemical analysis, and earlier measurements of Linde (1932) indicate a value of $1.59\ \mu\Omega\ \mathrm{cm\ (at\%)^{-1}}$.

5. Phase-shift analysis

A phase-shift analysis of transport data in a free-electron model has been succesfully applied to **Ag**Pd (Bekker and Zuiderbaan 1976) and Au–4d alloys (Myers *et al* 1980, Julianus *et al* 1984). This model has been extended to include crystal-field effects (Julianus and de Châtel 1984, to be referred to as JDC) and spin–orbit effects (Mrosan 1977, Lacueva *et al* 1982, to be referred to as LLF). To our knowledge, the simultaneous effect of the spin–orbit coupling and crystal fields on transport properties has not been treated theoretically. In what follows, we shall neglect the latter and find that a satisfactory interpretation of the resistivity and thermopower data is possible in terms of spin–orbit splitting alone.

Mrosan and LLF derived expressions for the resistivity along different lines. Mrosan dealt with the spin–orbit coupling in the free-electron model, deriving a transport relaxation time from

$$\frac{1}{\tau_{\mathrm{tr}}} = \frac{\hbar k}{mV} \int (1-\cos\theta)\left|\frac{\mathrm{d}\sigma}{\mathrm{d}\Omega}\right| \mathrm{d}\Omega \tag{2}$$

where V is the unit cell volume ($=a^3$, a being the lattice parameter). LLF, who discussed transport and EPR properties of noble metals with rare-earth impurities, considered two limiting cases: (i) the free 5d VBS and (ii) the cubic crystal-field-split 5d t_{2g} VBS. From the UPS spectra it is clear that the latter case is not applicable to **Ag**Pt. For the case (i), their results are at variance with those of Mrosan. Using the formalism developed by JDC, which does not make use of equation (2), we have verified (Julianus 1984) the latter result, which reads (Mrosan 1977, equation (5))

$$\frac{\rho}{c} = \frac{3\pi^3\hbar^5}{Ve^2m^2\varepsilon^2} \sum_{l=0}^{\infty} (l+1)[\rho_{l+}^{l+1+}(\varepsilon) + \rho_{l-}^{l+1-}(\varepsilon) + \rho_{l+}^{l+1-}(\varepsilon)]|_{\varepsilon=\varepsilon_F} = \frac{3\pi^3\hbar^5}{Ve^2m^2\varepsilon^2}\rho^0(\varepsilon)|_{\varepsilon=\varepsilon_F} \tag{3a}$$

where

$$\rho_{l+}^{l+1+}(\varepsilon) = \frac{l+2}{2l+3}\sin^2(\eta_{l+}(\varepsilon) - \eta_{l+1+}(\varepsilon)) \tag{3b}$$

$$\rho_{l-}^{l+1-}(\varepsilon) = \frac{l}{2l+1}\sin^2(\eta_{l-}(\varepsilon) - \eta_{l+1-}(\varepsilon)) \tag{3c}$$

$$\rho_{l+}^{l+1-}(\varepsilon) = \frac{1}{(2l+3)(2l+1)}\sin^2(\eta_{l+}(\varepsilon) - \eta_{l+l-}(\varepsilon)). \tag{3d}$$

Here η_{l+} and η_{l-} are the phase shifts corresponding to the states $j=l+\frac{1}{2}$ and $j=l-\frac{1}{2}$, respectively. The numerical value for the prefactor is $4.30\,\mu\Omega\,\mathrm{cm}\,(\mathrm{at}\%)^{-1}$ for Ag-based alloys.

The expression for A is found by using Mott's formula (Ziman 1960):

$$A=\frac{\pi^2 k_B^2}{3|e|}\frac{\partial \ln \rho}{\partial \varepsilon}\bigg|_{\varepsilon=\varepsilon_F}. \tag{4}$$

For scattering on d impurities it is reasonable to take the phase shifts for $l>2$ equal to zero. The energy dependence of s and p phase shifts can be neglected compared with that of the resonant d phase shift of the VBS:

$$\partial\eta_l/\partial\varepsilon=0 \qquad l=0,1 \tag{5a}$$

$$\partial\eta_j/\partial\varepsilon=\sin^2\eta_j/\Delta \qquad j=3/2,\,5/2\;(l=2). \tag{5b}$$

The last equation is a consequence of the assumed Lorentzian form of the resonance:

$$\tan\eta_j(\varepsilon)=\Delta/(\varepsilon_j-\varepsilon) \tag{5c}$$

where 2Δ is the FWHM of the VBS, which is found to be independent of j, and ε_j is the position of the spin–orbit-split VBS.

Substituting equations (3) into equation (4), and using equations (5), the expression for A becomes

$$A=\frac{\pi^2 k_B^2}{3|e|}\left(\frac{-2}{\varepsilon}+\frac{A^0(\varepsilon)}{\Delta\rho^0(\varepsilon)}\right)\bigg|_{\varepsilon=\varepsilon_F} \tag{6a}$$

where

$$A^0(\varepsilon)=[\tfrac{6}{5}\sin 2(\eta_{5/2}(\varepsilon)-\eta_1(\varepsilon))+\tfrac{9}{5}\sin 2\eta_{5/2}(\varepsilon)]\sin^2\eta_{5/2}(\varepsilon)$$
$$+[\tfrac{4}{5}\sin 2(\eta_{3/2}(\varepsilon)-\eta_1(\varepsilon))+\tfrac{6}{5}\sin 2\eta_{3/2}(\varepsilon)]\sin^2\eta_{3/2}(\varepsilon) \tag{6b}$$

and $\rho^0(\varepsilon)$ is defined by equation (3*a*). This result is again at variance with that given by LLF, partly due to their use of an incorrect expression for ρ and partly because they neglected the energy dependence of the prefactor in equation (3*a*). In an erratum, Hurd and Gordon (1970) have discussed this commonly made mistake which had led them to an incorrect expression for A (Hurd and Gordon 1968).

The Friedel sum rule (Friedel 1958) imposes a constraint on the phase shifts and can be written as

$$\Delta Z=\frac{2}{\pi}\eta_0(\varepsilon_F)+\frac{6}{\pi}\eta_1(\varepsilon_F)+\frac{4}{\pi}\eta_{3/2}(\varepsilon_F)+\frac{6}{\pi}\eta_{5/2}(\varepsilon_F). \tag{7a}$$

A correction for the size misfit of the atomic volumes of solute and solvent is made (Blatt 1957a, b). The Friedel sum used is therefore $\Delta Z=-0.85$. We find it convenient to represent the results in terms of partial screening charges, in which case the Friedel sum rule reads

$$-0.85=Z_0+Z_1+Z_{3/2}+Z_{5/2}. \tag{7b}$$

We are left with five independent variables, $Z_0, Z_1, Z_{3/2}, Z_{5/2}$ and Δ, and three equations, (3), (6) and (7). The information from the UPS spectra about the VBS enables us to obtain a solution to the transport data within our free-electron model. We neglected the crystal-field splitting indicated by the UPS spectra and identified the main maximum in the

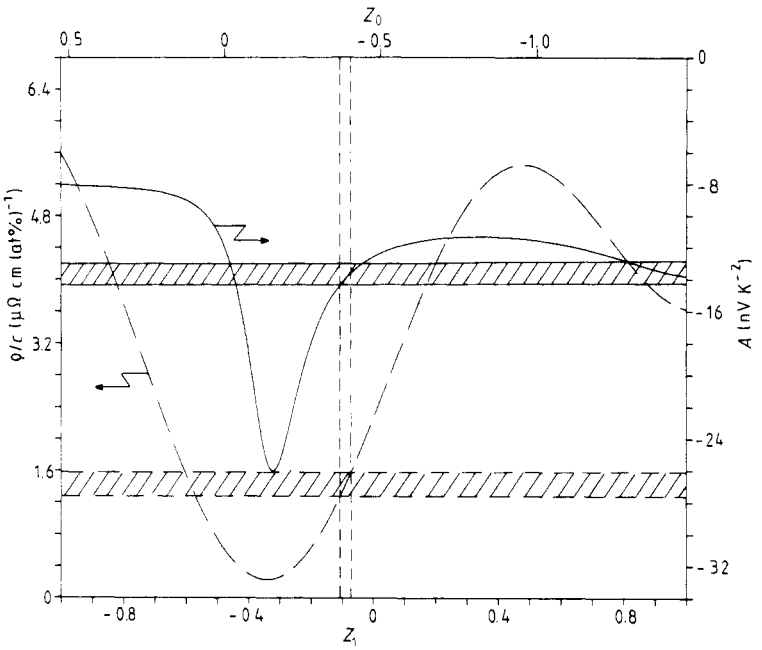

Figure 6. Resistivity (ρ/c) (broken curve) and TEP coefficient (A) (full curve) as functions of the partial screening charges Z_0 and Z_1. The values consistent with the experimental data lie within the shaded areas. The Friedel sum is $\Delta Z = -0.85$. The VBS parameters adopted from the UPS spectra are $E_{3/2} = -2.65$ eV, $E_{5/2} = -1.6$ eV and $2\Delta = 0.45$ eV.

structure closest to the Fermi energy with the $j = 5/2$ VBS. Using the position and FWHM values from the UPS measurements and the Friedel sum, we are able to plot ρ/c and A as functions of Z_0 or Z_1 (figure 6). The range of experimental resistivity values ($\rho/c = 1.45_5 \pm 0.13_5$ $\mu\Omega$ cm (at%)$^{-1}$) and thermopower coefficient ($A = -13.75 \pm 0.75$ nV K^{-2}) given in § 4.2 can be described by a unique set of screening charges:

$$Z_0 = -0.39 \pm 0.02 \qquad Z_1 = -0.09 \pm 0.02 \qquad Z_2 = Z_{3/2} + Z_{5/2} = -0.37_5.$$

The range for A is thereby confined to -14.0 ± 0.4 nV K^{-2}. The set of Z_0, Z_1 values is in excellent agreement with those derived from Knight shift measurements by Herberg and Voitländer (1980), who reported

$$Z_0 = -0.41_3 \pm 0.03 \qquad Z_1 = -0.09_5 \pm 0.04 \qquad Z_2 = -0.33 \pm 0.07$$

within a free-electron model, neglecting spin–orbit effects.

6. Conclusions

With high-resolution UPS we have shown that the Pt d state as an impurity in Ag retains its atomic structure. The UPS spectra are extremely well described with a quasi-atomic model resulting in three Lorentzian broadened levels. The spin–orbit coupling and crystal-field splitting parameters are determined from the position of the peak. The spin–orbit coupling is only slightly reduced from the atomic value.

Both the thermopower and the resistivity can be described by a unique set of phase

shifts, using the VBS parameters extracted from the UPS data, in a free-electron model including spin–orbit coupling and neglecting the crystal-field effects.

Acknowledgments

We wish to thank Professor Dr P F de Châtel for many helpful discussions and his continuous interest in this work. We are indebted to Dr A Myers of the University of Leeds for supplying the samples and sending his unpublished resistivity data, and to Dr J Kragten of the University of Amsterdam for chemical analysis of the samples. This investigation was supported by the Netherlands Foundation for Chemical Research (SON) with financial aid from the Netherlands Organization for the Advancement of Pure Research (ZWO).

References

Ballhausen C J 1962 *Introduction to Ligand Field Theory* (New York: McGraw-Hill)
Barber A J and Caplin A D 1975 *J. Phys. F: Met. Phys.* **5** 679–96
Bass J and Fischer K H 1982 *Numerical Data and Functional Relationships in Science and Technology, Group III: Crystal and Solid State Physics* vol. 15 (*Metals: Electronic Transport Phenomena*) subvol. a (Berlin: Springer)
Bekker F F and Hoogkamer T P 1976 *Physica* B **84** 67–76
Bekker F F and Zuiderbaan N 1976 *Physica* B **85** 113–21
Blatt F J 1957a *Phys. Rev.* **108** 285–90
—— 1957b *Phys. Rev.* **108** 1204–6
Bosch A 1982 *Thesis* University of Groningen
Friedel J 1958 *Nuovo Cimento* **7** 287–311
Guénault A M 1967 *Phil. Mag.* **15** 17–25
Herberg H and Voitländer J 1980 *Phys. Rev.* B **22** 5043–51
Hüfner S, Wertheim G K and Wernick J H 1975 *Solid State Commun.* **17** 1585–90
Hurd C M and Gordon E M 1968 *J. Phys. Chem. Solids* **29** 2205–19
—— 1970 *J. Phys. Chem. Solids* **31** 2586
Julianus J A 1984 *Thesis* University of Amsterdam
Julianus J A, Bekker F F and de Châtel P F 1984 *J. Phys. F: Met. Phys.* to be submitted for publication
Julianus J A and de Châtel P F 1984 *J. Phys. F: Met. Phys.* **14** 149–66
Kondo J 1965 *Prog. Theor. Phys.* **34** 204–9
Lacueva G, Levy P M and Fert A 1982 *Phys. Rev.* B **26** 1099–124
Linde J O 1932 *Ann. Phys., Lpz.* **15** 219–48
van der Marel D, Sawatzky G A and Julianus J A 1984 *Solid State Commun.* to be published
Moore C E 1949 *Atomic Energy Levels* NBS Circular No 467 (Washington, DC: US Government Printing Office)
Mrosan E 1977 *Phys. Status Solidi* b **80** K49–53
Myers A, Bekker F F and van Nassou H 1980 *J. Phys. F: Met. Phys.* **10** 461–9
Smith N V 1974 *Phys. Rev.* B **9** 1365–76
Smith P V 1981 *J. Phys. F: Met. Phys.* **11** 1063–73
Weightman P, Andrews P T, Stocks G M and Winters J 1983 *J. Phys. C: Solid State Phys.* **16** L81–7
Ziman J M 1960 *Electrons and Phonons* (London: Clarendon) p 397